Asymmetrical fed Calendula flower-shaped four-port 5G-NR band (n77, n78, and n79) MIMO antenna with high diversity performance

Tathababu Addepalli[1,2] (iD), T. Vidyavathi[3], K. Neelima[4], M. Sharma[5] (iD) and D. Kumar[6]

[1]Department of ECE, JNTUA, Anantapur, AP, India; [2]Department of ECE, Aditya Engineering College (A), Surampalem, Kakinada, AP, India; [3]Department of ECE, Gayatri Vidya Parishad College of Engineering (A), Visakhapatnam, AP, India; [4]Department of ECE, Sree Vidyanikethan Engineering College (A), Tirupati, AP, India; [5]Chitkara University Institute of Engineering and Technology, Chitkara University, Rajpura, Punjab, India and [6]Department of Physics and Electronics, Rajdhani College (University of Delhi), Delhi, India

Research Paper

Abstract

This research reports a four-port multiple-input-multiple-output (MIMO) antenna designed for 5G-NR band applications including n77: 3.30–4.20 GHz, n78: 3.30–3.80 GHz, and n79: 4.40–5.00 GHz. The proposed design is analyzed in two parts, one single-element asymmetrical fed Calendula flower-shaped antenna and the other four-port modified MIMO antenna with the connected ground. The evolution of the MIMO antenna is studied based on the characteristics and optimized single-element antenna. The measured 5G-NR bandwidth offers a very high matching of impedance for MIMO configuration and higher isolation in the same band. The MIMO antenna offers an average peak gain of 3.51 dBi with a radiation efficiency of more than 90%. The radiation patterns plotted at 3.51, 4.00, 4.50, and 5.00 GHz match with almost omni-directional and dipole patterns in H- and E-radiating planes respectively. The MIMO antenna also records good diversity performance (ECC, DG, CCL, MEG, and TARC) in n77, n78, and n79 5G bands.

Introduction

The channel capacity of the multiple-input-multiple-output (MIMO) antenna is increased due to the transmitter radiating the identical power and the receiver receiving it, and hence, there is no necessity for additional bandwidth [1]. This type of multiple radiating antennae suffers one major drawback which is maintaining isolation between the neighboring radiators which are closely packed. There can be different configurations of the MIMO antenna (2×2, 4×4) [1–35] which are designed for specific applications and ensure good isolation between them. The MIMO antennas [1–20] discuss the design methodology and isolation techniques used so that the interference between the neighboring radiators' field radiation is mitigated and hence, all the required results are preserved. A square patch with rectangular ground placed orthogonally maintains isolation of more than 30 dB [1] while a T-type stub attached to the ground between two adjacent radiators [2, 3, 12] and a tapered feed patch MIMO antenna [4, 8] observes better isolation by using rotated L-type strips. A funnel-shaped stub placed between shared ground [5], a rectangular-rotated L-type strip in the ground between two orthogonal radiating patches [6], and an etching pair of symmetrically-cut rectangular slots are the other reported techniques to achieve better isolation [7]. In an F-shape inverted antenna, a Swastik-shaped repetitive etched structure is applied to improve the isolation [9], and a short stub-loaded resonator with added T-shaped junction in between dual radiating patch [10] and novel elliptical type stub in-ground helps in achieving higher [11]. A unique pair of fractal stub [13, 15, 16] multiband MIMO antenna with a T-shaped stub on the ground [14] and the dual half-cut quasi self-complementary MIMO antenna utilizes no complex decoupling structure for isolation [17]; feather-type circular-shaped loaded radiator achieves isolation by placing the two identical radiators orthogonally or adjacent to each other [18, 19] and a T-type stub etched with semi-circular slot also helps in maintaining higher isolation between two radiating elements placed adjacent to each other [20]. The above-discussed MIMO antenna is of 2×2 configuration and also different techniques are applied to achieve better isolation in a four-port MIMO configuration. A four-semielliptical MIMO antenna with an asymmetric coplanar strip placed in an orthogonal fashion occupying a size of $48 \times 52 \text{ mm}^2$ on an FR4 substrate requires no additional isolation element [21]. A MIMO antenna for automative application which is interlocked with a four-radiating patch achieves higher isolation in a bandwidth of 2.80–9.50 GHz [22]. Radiation pattern and polarization diversity are achieved in four pairs of microstrip fed antenna which also consists of dual-concentric annular slots [23, 24] and five concentric stubs placed between four radiators [25]; a defected ground structure monopole of 4×4

configuration uses no isolation element as the inter-spacing between them achieves higher isolation [26] and by maintaining the spacing of <0.05λ between radiators isolation of more than 16 dB is achieved [27]. Three MIMO antenna configurations [28–30, 32, 33] with four radiating patches utilize no decoupling structures and a fan-shaped parasitic structure between the four-radiating patch achieves better isolation [31]. A three-layered MIMO antenna offers high diversity performance with isolation <−20 dB [34] and four square-patch placed exactly at the center of the edges with defected ground records isolation of <−37.50 dB in the operating band of interest [35].

This paper reports a 4 × 4 MIMO antenna configuration designed for 5G-NR bands applications which include n77, n78, and n79. The reported design consists of a Calendula-shaped radiating patch which is fed asymmetric using a microstrip. The four-radiating patch which also consists of respective rectangular etched ground and an attached rectangular provides good impedance matching and interconnected ground with strip results in higher isolation between them, thereby providing a better platform for diversity performance. The MIMO design is carried out by first designing a single radiating antenna and then modifying the same to the MIMO configuration which is discussed below.

Proposed antenna configuration and antenna evolution (single radiating patch)

This research discusses the evolution of the proposed single-element antenna which is modified to work with a four-port configuration and mitigates all the demerits possessed by a single radiating patch. Figure 1 shows the complete configuration of the proposed unit element antenna with a radiating patch resembling Calendula flower and rectangular ground etched with the rectangular slot. Figure 1(a) shows the perspective view of the antenna is fabricated on an FR4 substrate for the design of the proposed antenna. Figure 1(b) shows the detailed dimensions which are optimized by using an EM simulator. Also, it can be observed that the radiating patch is fed by an asymmetric 50 Ω microstrip line. The partial rectangular ground which is printed on the opposite plane of the substrate is etched with a rectangular slot behind the microstrip line. Figure 1(c) represents the detailing of the Calendula flower leaves and these leaves are aligned at different angles concerning origin ($E1 = 165°$, $E2 = 015°$, $E3 = 90°$, $E4 = 105°$, and $E5 = 70°$ (anticlockwise direction)). All the optimized dimensions shown in Fig. 1 are recorded in Table 1 given below.

The next step is to study the evolution of the proposed antenna which is shown in Fig. 2. Figure 2(a) depicts a circular patch antenna with the ground on the opposite plane containing the patch. This antenna #1 exhibits very poor matching of the impedance as observed in Fig. 2(e). The improvement of the impedance is noted by modifying antenna #1 to antenna #2 where the circular patch is etched by a circular slot and the partial ground is etched with a rectangular slot which is shown in Fig. 2(b). This modification improves the matching of impedance and the partial 5G NR bands are achieved. Further antenna #3 shows the addition of three fractal leaves with the patch connected to asymmetric feed. The lower bandwidth is improved when compared with the previous version. The final version of the antenna shown in Fig. 2(d) which is antenna #4 achieves all the 5G NR bands including n77, n78, and n79 which is the objective of the design. The modification includes the addition of two more cornered

leaves and a rectangular stub attached to the ground providing an impedance bandwidth of 3.18–5.53 GHz.

Study of key parameters affecting the bandwidth and surface current distribution

The proposed single-element antenna discussed in section "Proposed antenna configuration and antenna evolution (single radiating patch)" was the optimized version shown in Fig. 1. However, the key parameters which are optimized including *Wf*, axial ratio, *L2*, and *Lg* offer a vital role in the matching of the impedance and designing of the antenna, thus, change in their respective physical length does affect the operating bandwidth to a larger extent. These effects are seen by studying the parametric study shown in Fig. 3. The width of the microstrip, *Wf* is calculated by following equations

$$Wf = \left(\frac{7.48 \times h}{e^{Zo\frac{\sqrt{\varepsilon r + 1.41}}{87}}} \right) - 1.25 \times t, \tag{1}$$

$$Zo = \frac{120\pi}{\sqrt{\varepsilon eff \left[\frac{Wf}{h} + 1.393 + \frac{2}{3}\ln\left(\frac{wf}{h} + 1.444 \right) \right]}}, \tag{2}$$

$$\varepsilon eff = \frac{\varepsilon r + 1}{2} + \frac{\varepsilon r - 1}{2} \left[1 + 12\frac{h}{wf} \right]^{\frac{-1}{2}}. \tag{3}$$

Here *Zo* is the impedance (Ω), *Wf* is the width of microstrip (mm), *t* is the trace width (mm), *h* is the height of the dielectric material used in this design, *εr* is the permittivity of the microwave substrate used.

As per the observations from Fig. 3(a), the width of the microstrip line changes the impedance of the feed which is governed by three equations, equations (1)–(3). The impedance of the feed line is designed for 50 Ω and the variation of width *Wf* also changes the impedance which in turn affects the overall impedance of the antenna. The values for *Wf* are changed from 2.10 to 2.50 mm, achieving the required bandwidth, but more matched impedance is observed for *Wf* = 2.30 mm with S11 = −44.86 dB at 4.00 GHz. Similarly, the partial ellipse used in the design with axial ratio = 2.0 shown in Fig. 3(b) also provides the required impedance bandwidth of 3.18–5.51 GHz with corresponding S11 = −44.86 dB at 4.00 GHz. The variation of *L2* which is the height of the etched rectangular slot on the ground observes a larger deviation of the S11 parameter recorded in Fig. 3(c). For *L2* = 3.00 mm which is an optimized value that achieves the 5G NR bands. Another important parameter *Lg*, which is the length of the ground, observes very poor matching of impedance for *Lg* = 11.50 mm and deviation of center resonance frequency to 4.48 GHz for *Lg* = 13.50 mm. After optimization, for *Lg* = 12.50 mm, the impedance bandwidth covers n77, n78, and n79 bands with S11 = −44.86 dB at 4.00 GHz.

The illustration of the surface current density at 3.30, 3.50, 4.00, 4.50, 4.80, and 5.00 GHz is shown in Fig. 4. Figures 4(a) and 4(b) show the distribution of surface current for 3.30, 3.50, and 4.00 GHz which covers the n77 and n78 bands. From the observations, the electric current is strongly distributed on the portion of microstrip and rectangular stub attached to the ground and confirms that these three-antenna areas form part of the
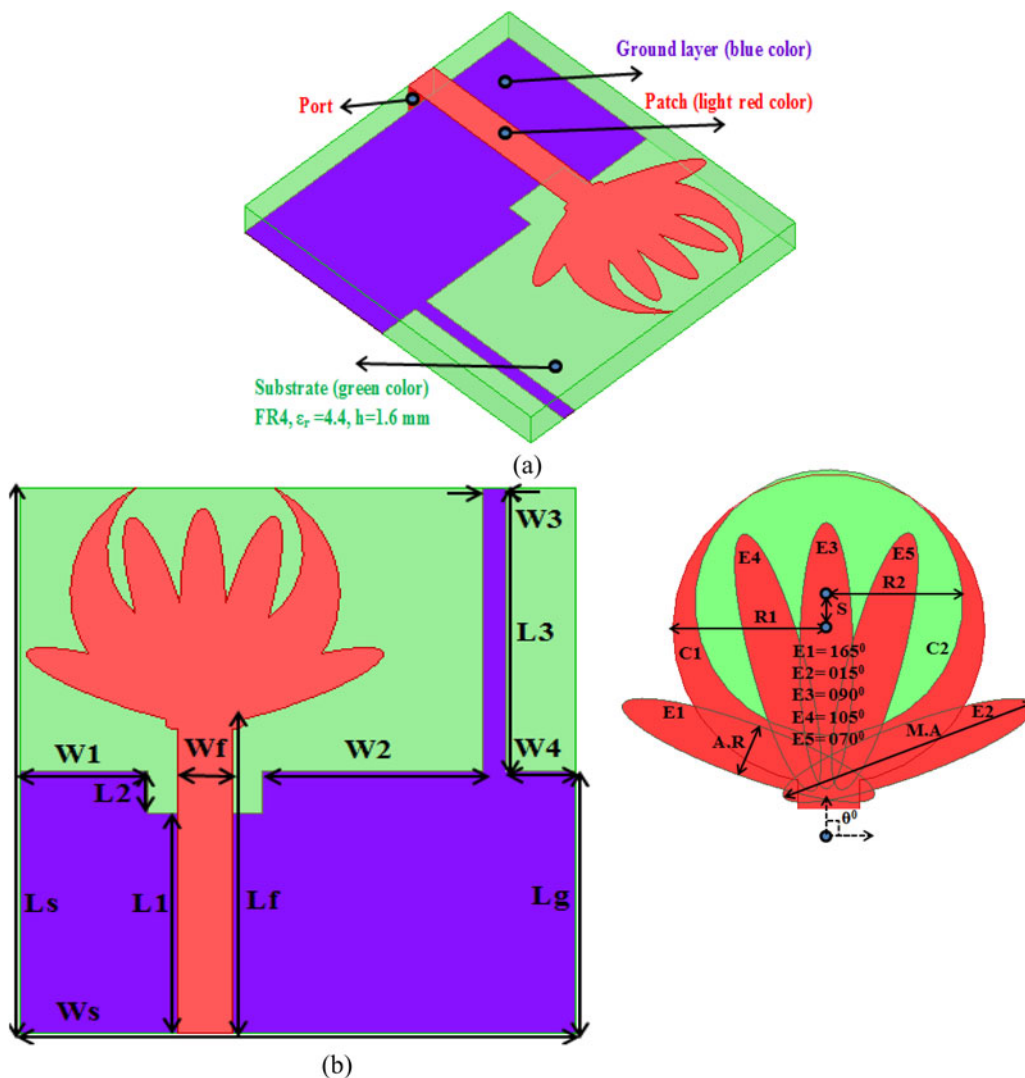
Fig. 1. Proposed 5G-NR antenna design with single radiation patch; (a) perspective view, (b) front view with a magnified patch.

radiating structure. It can also be depicted from Fig. 3(d) that the length of the ground does affect the matching of the impedance. Figures 4(d)–4(f) show the simulated current density distribution for 4.50, 4.80, and 5.00 GHz respectively for the n79 band. The same observations are noted that the surface current density is maximum within the feedline. For the remaining area of the antenna structure, the distribution of surface current is maximum, thereby ensuring all the input signals are radiated.

Modified 4 × 4 MIMO antenna (without and with stub)

The high throughput in the limited bandwidth environment is solved in multiple antenna configurations or MIMO systems. The demand for the faster transmission of higher data concerning time lead to the evolution of the MIMO antenna maintaining enhanced bandwidth/throughput of the data under different conditions including interference, fading of the signal, and multipath followed by signal at the receiver side. It is known from the Shannon–Hartley theorem [36] that the capacity of the channel is given by

$$C = BW \log_2(1 + SNR), \tag{4}$$

where C is the channel capacity, BW is the bandwidth, and SNR is a signal-to-noise ratio.

From above equation (4), it can be concluded that the channel capacity can be increased by increasing more number of radiating antennas rather than a single one. A MIMO channel capacity is calculated by

$$C_{MIMO} = N \times BW \log_2(1 + SNR). \tag{5}$$

Equation (5) suggests that increasing the number of radiating elements rather than increasing channel SNR which ends up in marginal gains increases the channel bandwidth and hence higher throughput is achieved.

Based on the above concept, a 4 × 4 MIMO antenna configuration is developed which is the modified version of the single radiating antenna discussed in previous sections. All the key results corresponding to MIMO configuration including bandwidth, diversity performance, and far-field results are discussed below.

Figures 5(a)–5(d) show the design of the 4 × 4 MIMO antenna which is the modified version of the antenna shown in Fig. 1.

Figure 5(a) shows the reflection coefficient (S11 in dB) curves with a 4 × 4 MIMO antenna configuration. The unit cell or single

Table 1. Proposed single and four-element 5G radiators parameter with values

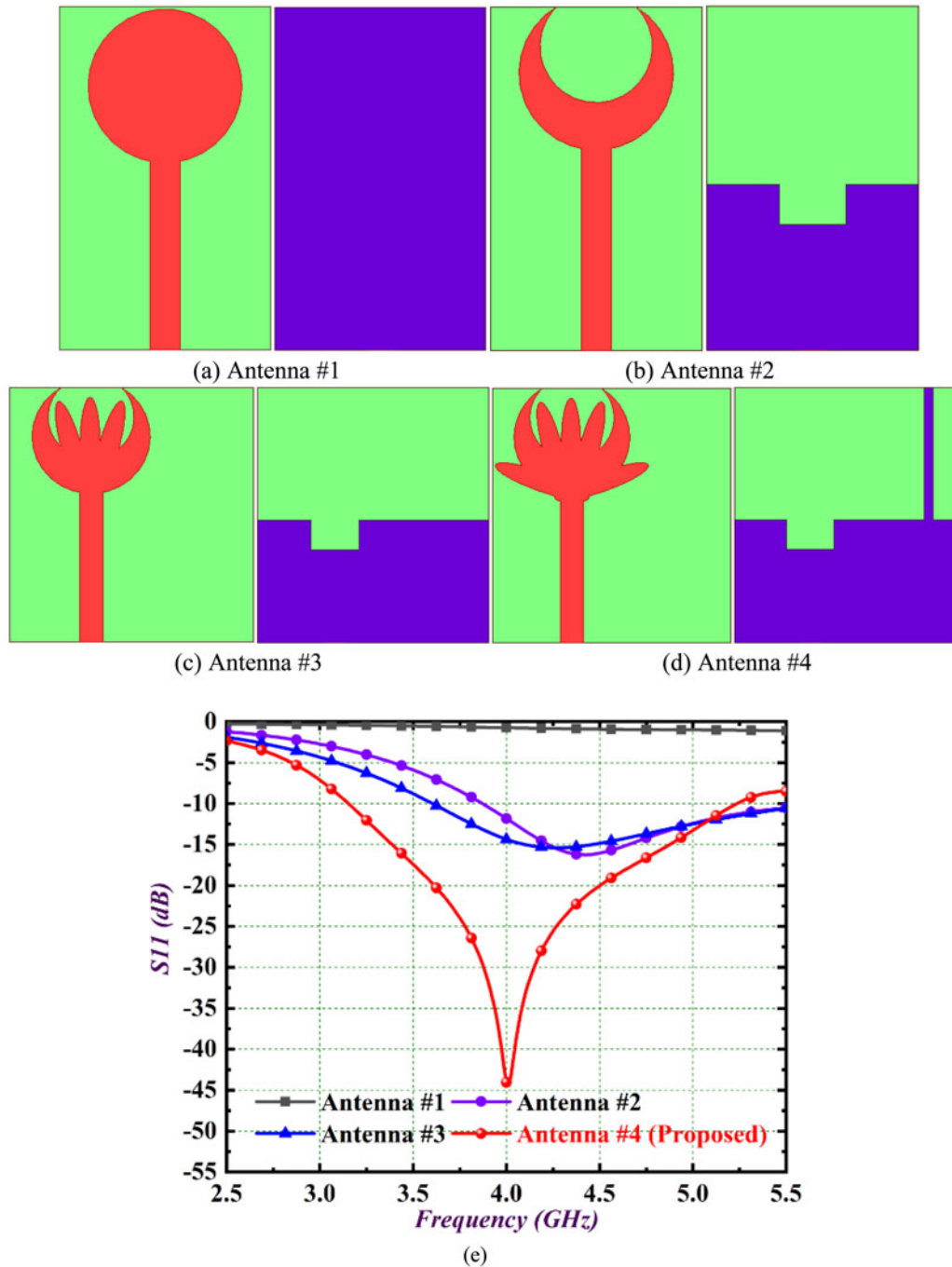| Parameter	Ls	Ws	Lg	Lf	Wf	L1	L2	L3
Value (mm)	26	24	12.5	14.8	2.3	9.5	3	13.5
Parameter	L4	L5	W1	W2	W3	W4	W5	W6
Value (mm)	1.75	1	5.5	9.5	1	3	8	6
Parameter	Ws1	Ls1	R1	R2	S	A.R	M.A	h
Value (mm)	58	58	5.8	4.2	2.2	2	10	1.6

Fig. 2. Evolution of the antenna (a) Antenna #1 (b) Antenna #2 (c) Antenna #3 (d) Antenna #4 (e) S11 result of Antenna#1–Antenna#4.
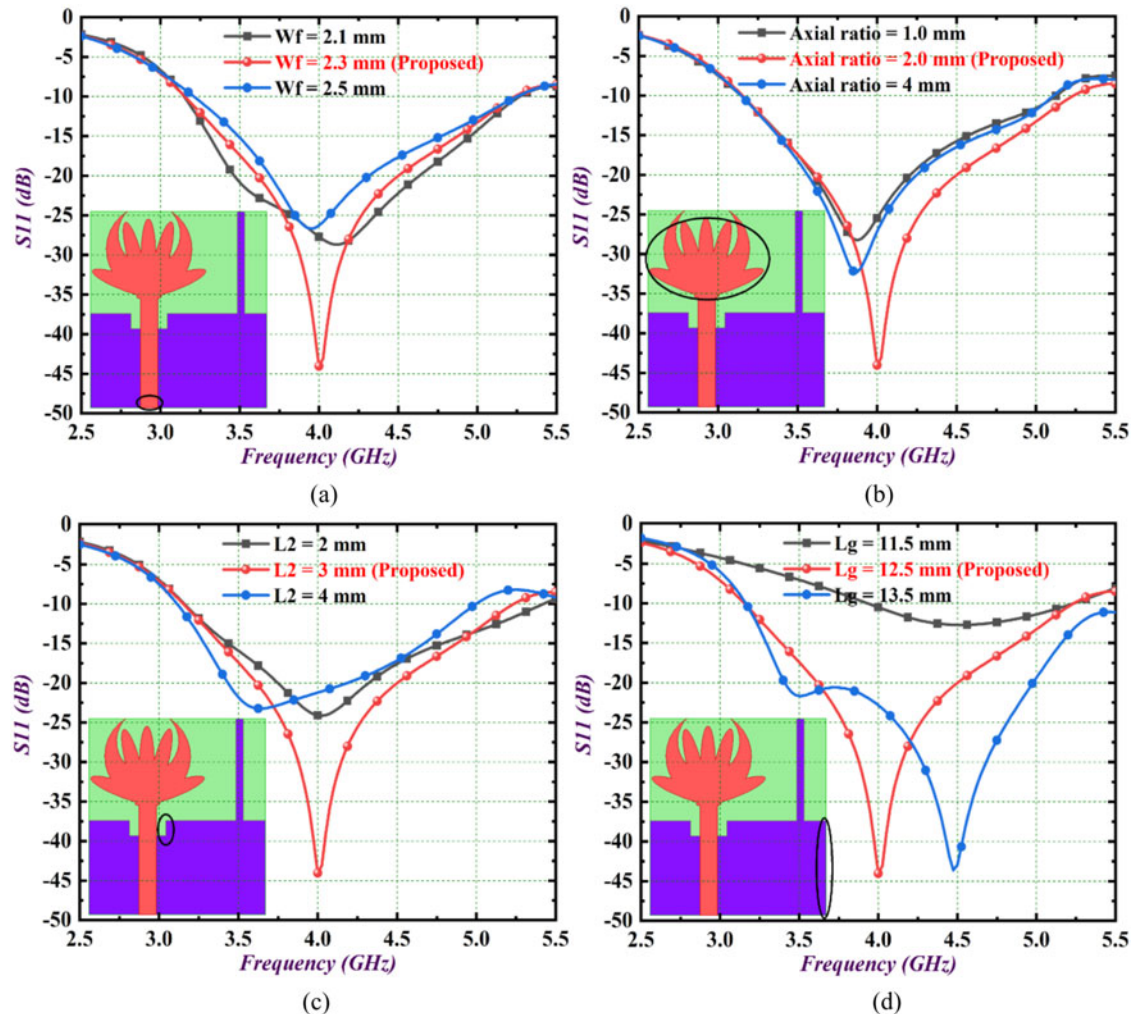
Fig. 3. Parametric analysis on; (a) feed width (*Wf*), (b) axial ratio (*A.R*), (c) truncated ground slot length (*L2*), (d) truncated ground length (*Lg*).

radiating antenna is placed in orthogonal sequence with their respective ground to achieve spatial diversity. Figure 5(a) shows the simulated *S*11 curves for different sizes of the antenna (54 × 54, 56 × 56, 58 × 58, and 60 × 60 mm²). The optimized size of the antenna with 60 × 60 mm² achieves the required 5G bands and also the center frequency. It is worth noting that there is no decoupling structure used, but Fig. 5(b) which shows the transmission coefficient curve between port 1-port 2 and port 1-port 4 observes poor isolation between them due to the reason that they are placed adjacently. Figure 5(c) which shows the isolation graph (*S*31 in dB) between port 1-port 3 records better values of isolation in the operating band suggesting that these two radiating patches are not adjacent but are diagonally placed in an orthogonal fashion. Also, the proposed antenna as observed in Fig. 5(c) shows better *S*13 results. Figure 5(d) compares the reflection and transmission coefficients of port 1 concerning port 2, port3, and port 4. The required bandwidth for 5G bands is achieved but the matching of impedance is poor and can be further improved when a decoupling structure is used. Also, the *S*31 shows good isolation, but *S*21 and *S*41 offer poor isolation between them and need to be improved.

Figure 6 shows the distribution of surface current density for a four-element 5G radiator with the isolated ground for frequencies 3.30, 3.50, 4.00, 4.50, 4.80, and 5.00 GHz. This simulation is

obtained by exciting port 1 and matching all the remaining ports (port 2, port 3, and port 4) with the matched impedance of 50 Ω. As per the observations from all the six figures shown in Fig. 6 for different frequencies, it can be observed that the interference between the adjacent radiating antennas is more while the antenna placed diagonally has less interference which is already shown in Figs 5(c) and 5(d). The above-discussed results for MIMO antenna will not result in very good diversity performance, and hence further modification or addition of decoupling structure becomes necessary.

The 4 × 4 MIMO antenna discussed in Fig. 5 inherits demerits such as poor isolation and hence poor diversity performance. This problem is overcome in the proposed 4 × 4 MIMO antenna configuration shown in Fig. 7. Figure 7(a) shows the prototype of the proposed 4 × 4 MIMO antenna configuration with a decoupling structure connected to all the grounds. The modification of the MIMO antenna ensures better isolation between all the ports which was not available in the earlier proposed MIMO design. The rectangular strip which is interconnected with the ground as shown in Fig. 7(b) ensures good impedance matching for the desired n77, n78, and n79 bands as shown in Fig. 7(d). It can be observed that the simulated *S*11 parameter offers the maximum value of −44.68 dB at 4.18 GHz, while the measured values are −50.28 dB at 4.52 GHz. In both the simulated and measured
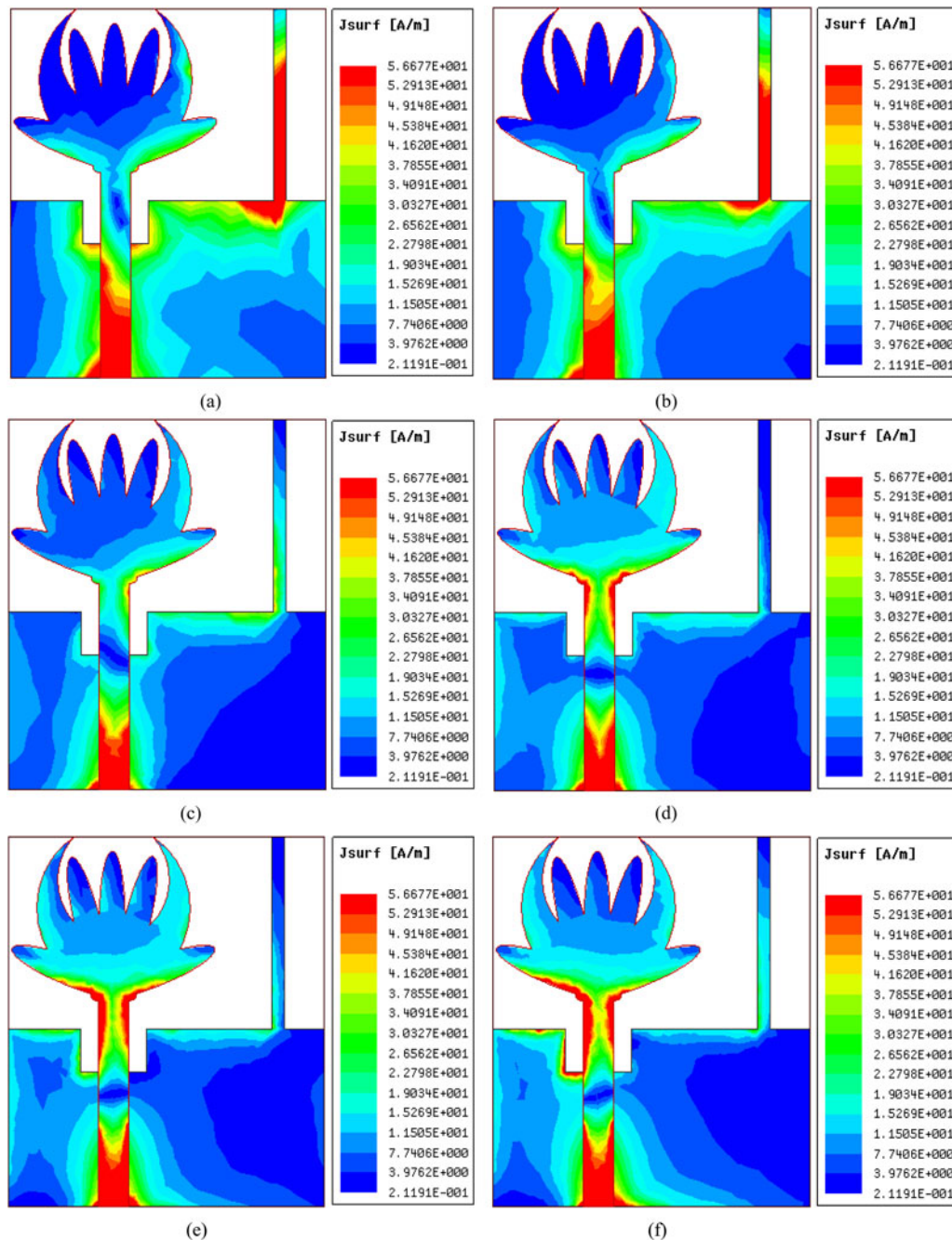
Fig. 4. Surface current distribution of 5G single radiator at various frequencies; (a) at 3.30 GHz, (b) at 3.50 GHz, (c) at 4.00 GHz, (d) at 4.50 GHz, (e) at 4.80 GHz, (f) at 5.00 GHz.

results comparison, the MIMO antenna covers all the 5G bands. Similarly, the proposed MIMO antenna also offers better isolation of more than −15 dB for both simulated and measured results.

Figures 7(d)–7(i) show the distribution of surface current for 3.30, 3.50, 4.00, 4.50, 4.80, and 5.00 GHz. Port 1 corresponding to antenna #1 is excited while all the remaining ports (port 2, port 3, and port 4) are terminated with a matched impedance of 50 Ω. The transmission coefficients shown in Fig. 7(c) offer isolation of more than −15 dB and this is due to the reason that the additional decoupling structure used in the ground provides an additional path for the flow of current and hence prevents the

interaction between all the remaining radiating antennas, thereby reducing the interference which was observed for MIMO antenna without decoupling structure.

Diversity performance

There are different diversity schemes such as space diversity, frequency diversity, angle diversity, time and multiple path diversity, and polarization diversity. The fading of the two signals will differ when two or more radiating antennas are separated by a minimum distance of $0.5\lambda o$ (where λo is the operating wavelength
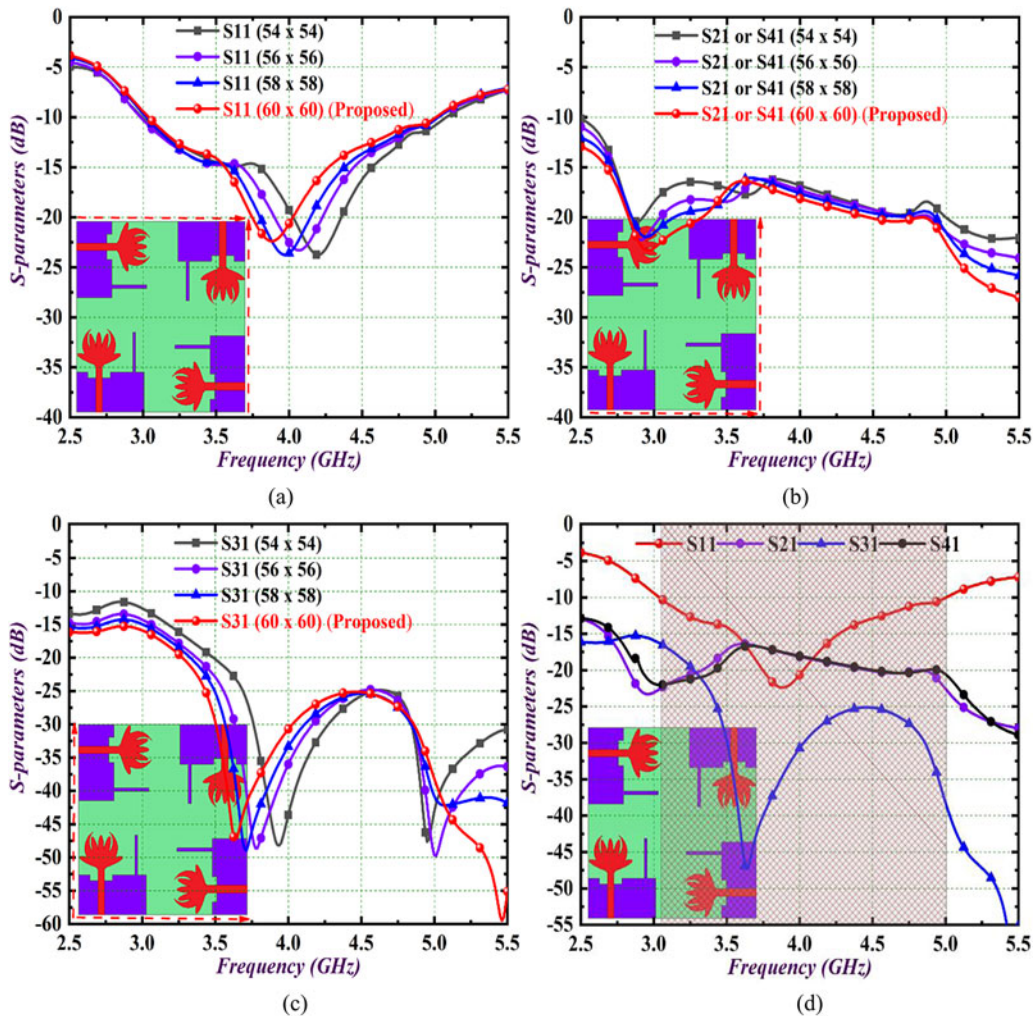
Fig. 5. Parametric analysis on substrate of isolated ground; (a) *S*11 values, (b) *S*21 or *S*41 values, (c) *S*31 values, (d) *S*-parameters of 60 × 60 mm² size 5G radiator with isolated ground.

corresponding to the frequency of 4.00 GHz in the proposed 4 × 4 MIMO antenna configuration (Table 2).

Envelope correlation coefficient (ECC) which is a very important parameter of diversity performance is calculated by using either a far-field radiation pattern or using scattering-parameter. Calculation of ECC from *S*-parameter makes assumptions that

$$ECC_{m \times n} = \frac{|S_{11}^* S_{12} + S_{21}^* S_{22}|^2}{(1 - |S_{11}|^2 - |S_{21}|^2)(1 - |S_{22}|^2 - |S_{12}|^2)}. \qquad (7)$$

For the four-port MIMO antenna configuration, ECC is evaluated by

$$ECC_{m \times n} = \frac{|S_{11}^* S_{12} + S_{12}^* S_{22} + S_{13}^* S_{32} + S_{14}^* S_{42}|^2}{(1 - (|S_{11}|^2 + |S_{21}|^2 + |S_{31}|^2 + |S_{41}|^2))(1 - (|S_{12}|^2 + |S_{22}|^2 + |S_{32}|^2 + |S_{42}|^2))}. \qquad (8)$$

all the signals which are fed to the antenna are uniform spread, as well as all the radiation elements are well matched and possess no loss. The following equations show the calculation of ECC using radiation patterns concerning fields radiated and *S*-parameter (2 × 2 and 4 × 4 MIMO) [3, 27]

$$ECC_{m \times n} = \frac{\left| \iint \overrightarrow{F_m}(\theta, \phi) . \iint \overrightarrow{F_n}(\theta, \phi) \, d\Omega \right|^2}{\iint \left| \overrightarrow{F_m}(\theta, \phi) \right|^2 d\Omega \iint \left| \overrightarrow{F_n}(\theta, \phi) \right|^2 d\Omega}, \qquad (6)$$

In equation (6), *Fm* and *Fn* have radiated fields of the *m*th and *n*th antennas. For the ideal MIMO array, the ECC is zero, but for practical cases, these values are expected to be <0.50.

The effective diversity in the communication channel is given by the diversity gain which shows the dissimilarity between the time-average SNR signals. This compares the diversity of several radiating antennae when compared with the single antenna system. The DG which is evaluated by equation (9) is related to
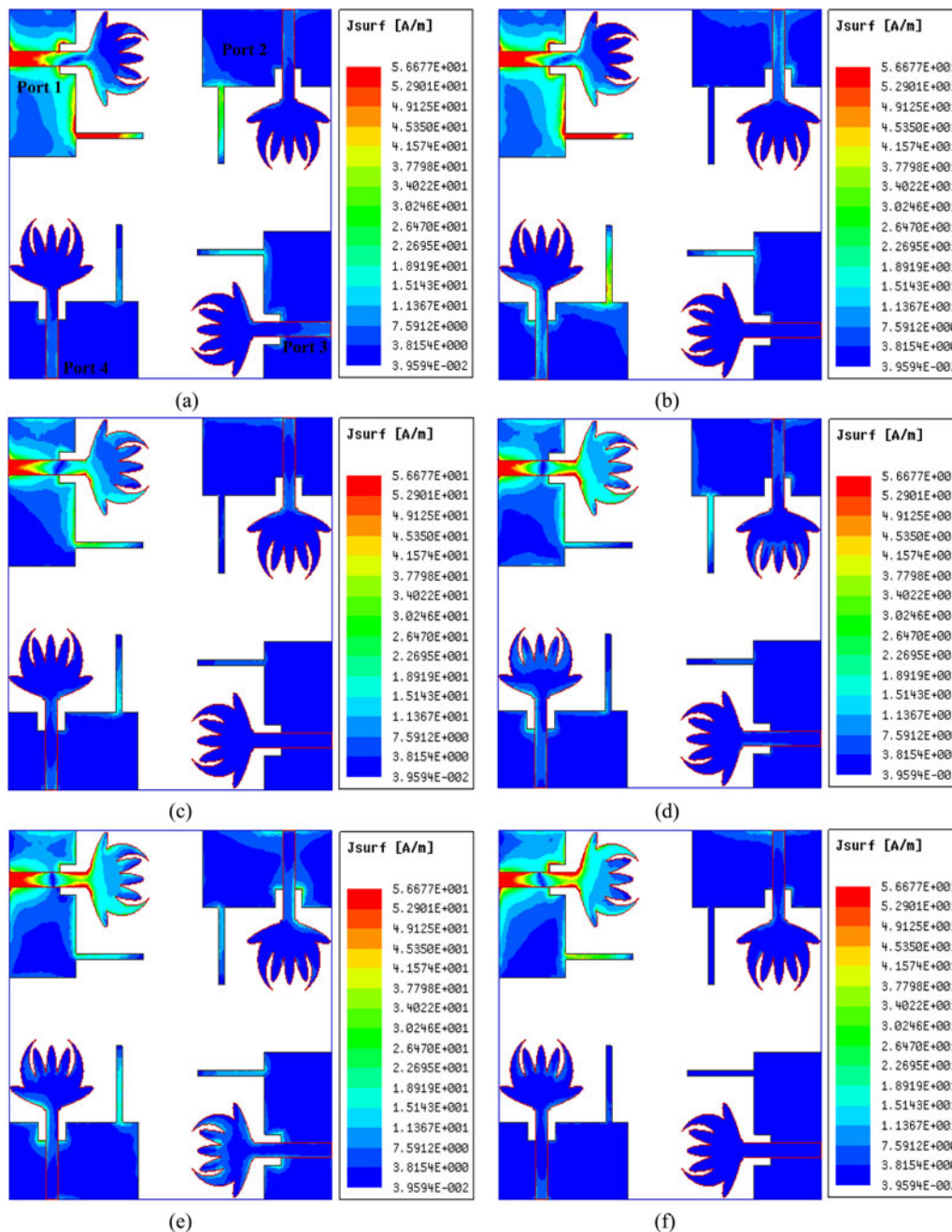
Fig. 6. Surface current distribution of four-element 5G radiator isolated ground at various frequencies when port 1 is excited; (a) at 3.30 GHz, (b) at 3.50 GHz, (c) at 4.00 GHz, (d) at 4.50 GHz, (e) at 4.80 GHz, (f) at 5.00 GHz.

ECC as given by

$$DG_{m \times n} = \sqrt{1 - ECC_{m \times n}^2}. \qquad (9)$$

The values of directive gain (DG) should be ideally 10 dB, and in the proposed antenna, these values are approximately 10 dB as noted in Fig. 8(b).

The capacity of the channel signifies the efficient transmission of the signal with no distortion or loss of data bits in the communication environment. However, the ideal condition is not achieved, and hence channel capacity loss (CCL) has to be evaluated which is given by the following equations

$$Channel\ capacity\ loss_{m \times n} = -\log_2(\Omega^{MIMO}), \qquad (10)$$

where

$$\Omega^{MIMO} = \begin{bmatrix} \Omega_{11} & \Omega_{12} \\ \Omega_{21} & \Omega_{22} \end{bmatrix}, \qquad (11)$$

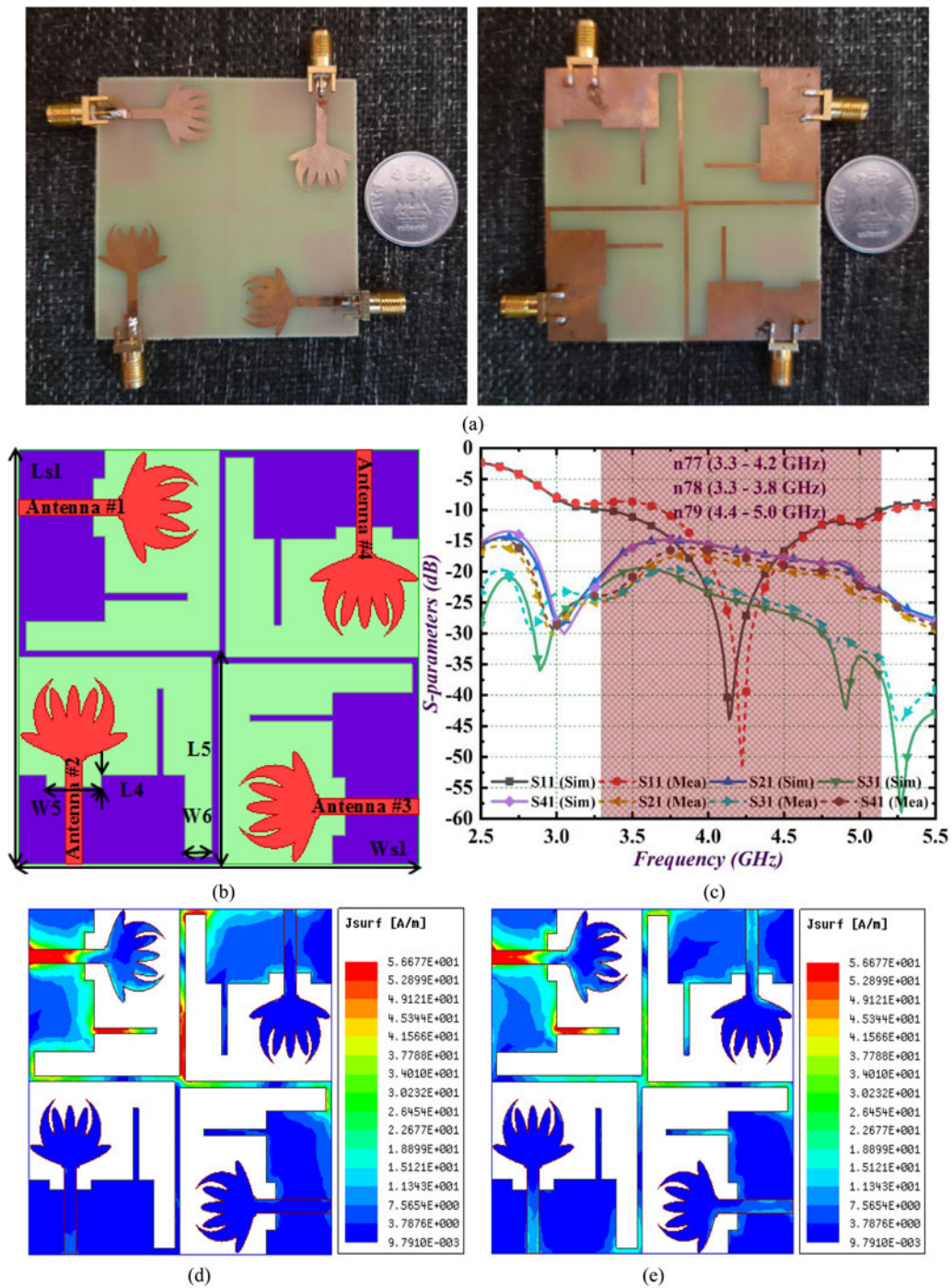$$\Omega_{11} = 1 - [|S_{11}|^2 + |S_{12}|^2], \qquad (12)$$

Fig. 7. (a) Prototype of 4 × 4 MIMO antenna with decoupling structure; (b) simulation snapshot; (c) simulated and measured S-parameters; (d)–(i) surface current density distribution at 3.30, 3.50, 4.00, 4.50, 4.80, and 5.00 GHz.

$$\Omega_{22} = 1 - [|S_{22}|^2 + |S_{21}|^2] \tag{13}$$

$$\Omega_{12} = -[S_{11}^* S_{12} + S_{21}^* S_{12}], \tag{14}$$

$$\Omega_{21} = -[S_{22}^* S_{21} + S_{12}^* S_{21}]. \tag{15}$$

The maximum allowable CCL values or ideally CCL < 0.40 b/s/Hz and in the proposed 4 × 4 MIMO antenna configuration, the values of CCL are 0.04 b/s/Hz which are better than 10 times the ideal values as observed in Fig. 8(c).

The antenna receiving averaged signal is computed by the diversity parameter known as mean effective gain (MEG) and is defined as the ratio of the power received by the receiving antenna to the total power which is incident on it. The MEGs are calculated between any two antennas by generalized formula given
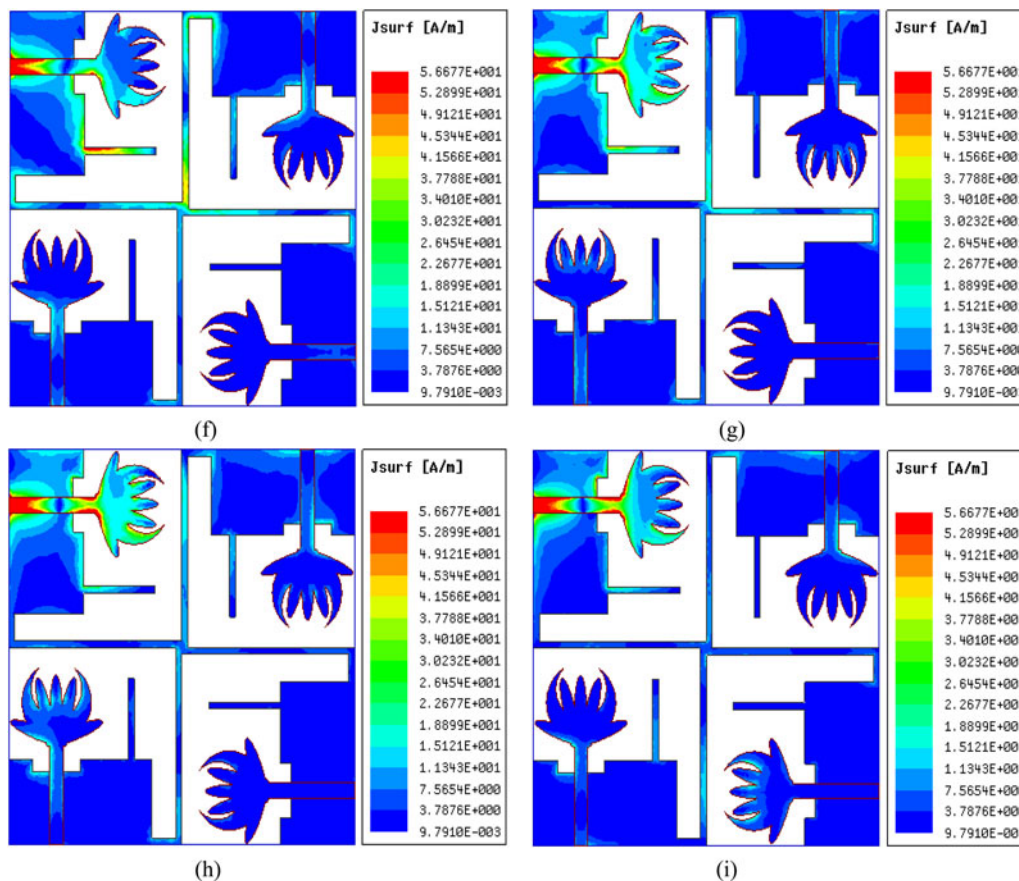
(f)

(g)

(h)

(i)

Fig. 7. Continued.

Table 2. Comparison of $S11$, $S21$ (or) $S41$, and S31 of 5G radiators

5G radiator/parameter	S11 (GHz)	S21 (or) S41 (dB)				S31 (dB)			
Single radiator (26 × 24)	3.16–5.22	NA				NA			
Four-element radiator with isolated ground (60 × 60)	3.05–5.01	At 3.5 GHz	At 4.0 GHz	At 4.5 GHz	At 5.0 GHz	At 3.5 GHz	At 4.0 GHz	At 4.5 GHz	At 5.0 GHz
		17.2	18.1	20.1	22.5	29.6	30.7	25.1	38.1
Four-element radiator with connected ground (58 × 58)	3.31–5.13	At 3.5 GHz	At 4.0 GHz	At 4.5 GHz	At 5.0 GHz	At 3.5 GHz	At 4.0 GHz	At 4.5 GHz	At 5.0 GHz
		15.9	15.6	17.6	21.9	19.5	23.3	26.7	33.7

for the mth and nth antenna

$$MEG_m = 1 - |S_{mm}|^2 - |S_{mn}|^2, \qquad (16)$$

$$MEG_n = 1 - |S_{nn}|^2 - |S_{nm}|^2. \qquad (17)$$

The ratio calculates the MEG which is given by

$$\frac{MEG_m}{MEG_n} = \frac{1 - |S_{mm}|^2 - |S_{mn}|^2}{1 - |S_{nn}|^2 - |S_{nm}|^2}. \qquad (18)$$

For the proposed antenna, MEGs calculated for antenna #1-antenna #2, antenna #1-antenna #3, and antenna #1-antenna #4 were simulated and measured values are plotted in Fig. 8(d). As per the observations, the ratio of MEG values is approximately −3.0 dB for both simulated and measured values.

In MIMO antenna configuration, the radiating elements are closely placed to each other and are operated at the same time, but this arrangement of radiating antennas also affects the performance in terms of interference. This suggests that the S-parameters obtained for the MIMO antenna only do not ensure the merit of interference, and hence a new parameter called total-active-reflection-coefficient (TARC) needs to be evaluated. This parameter is defined as the "square root of the ratio of
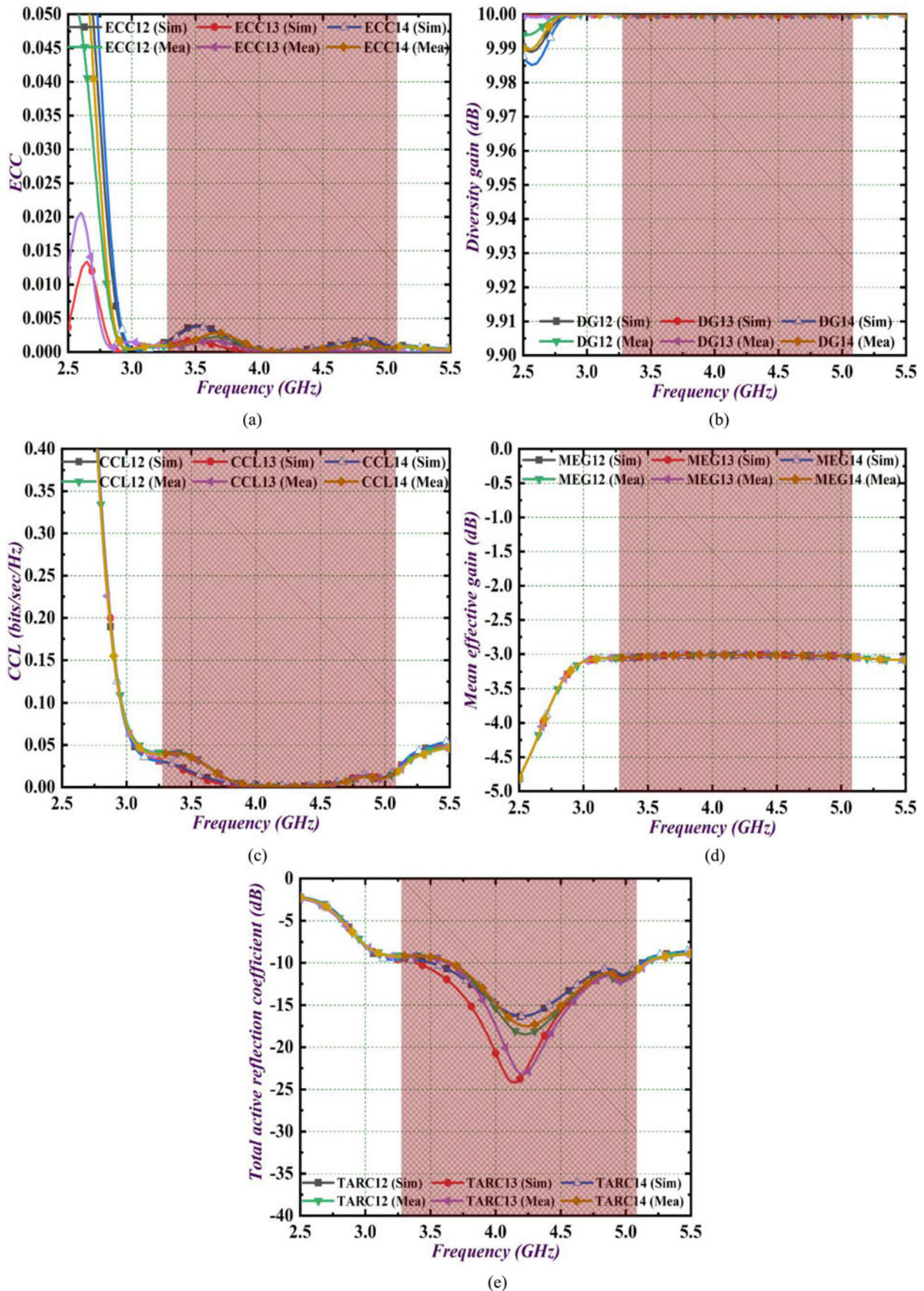
Fig. 8. Diversity performance; (a) ECC$_{4\times4}$ (simulated and measured), (b) DG$_{4\times4}$ (simulated and measured), (c) CCL$_{4\times4}$ (simulated and measured), (d) MEG$_{4\times4}$ (simulated and measured), (e) TARC$_{4\times4}$ (simulated and measured).
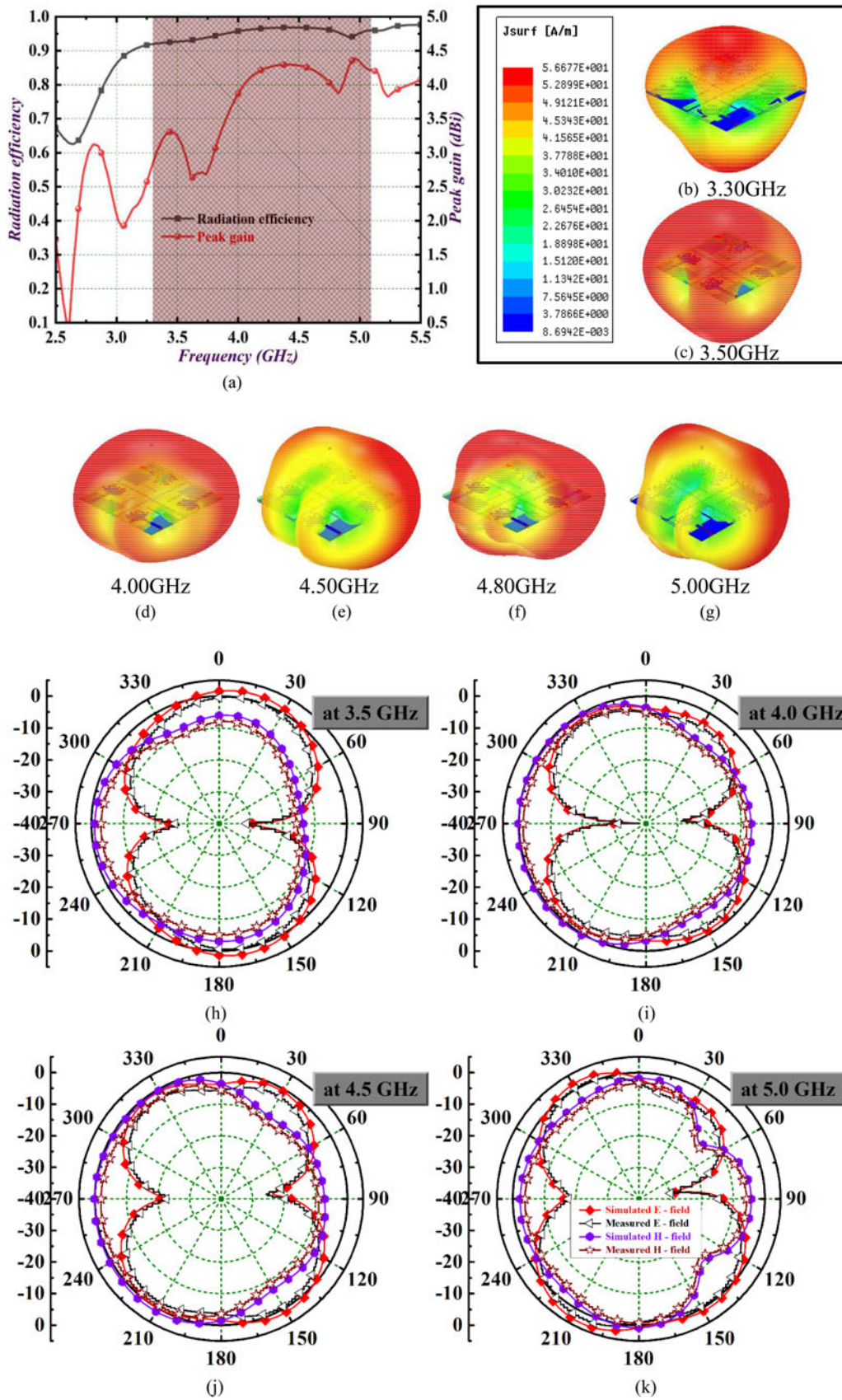
Fig. 9. Far-field result discussion; (a) radiation efficiency and peak gain, (b)–(g) 3D radiation pattern, (h)–(k) 2D radiation pattern.

Table 3. Comparison of the proposed work with the latest reported articles

Ref. year	Con.	Size (mm × mm)	Bandwidth (GHz)	Isolation (dB)	ECC	DG (dB)	CCL b/s/Hz	MEG (dB)	TARC (dB)	Substrate
[1] 2021	2 × 2	24 × 24	3.89–11.97	<−25.0	<−0.4	>9.95	<0.38	–	<−30	Rogers RT Duroid 5880
[5] 2018	2 × 2	15 × 26	3.10–35.0	<−20.0	<−0.001	>9.95	–	–	<−30	FR4
[9] 2021	2 × 2	50 × 100	5.20–6.00	<−25.0	–	–	–	–	<−4.44	FR4
[12] 2020	4 × 4	35 × 36	2.60–12.20	<−17.0	<−0.012	>9.9993	–	–	<−6	FR4
[15] 2020	2 × 2	41 × 99.4	4.30–11.60	<−15.8	<−0.008	>9.99	<0.40	<3.0	–	FR4
[16] 2021	3 × 3	πr^2 (r = 32 mm) 100.48	3.33–3.58	<−10.0	<−0.4	>9.96	–	<3.0	<−5	F4BME
[20] 2020	2 × 2	24 × 32	3.00–11.0	<−20.0	<−0.005	–	<0.04	<3.0	<−10	FR4
[21] 2021	4 × 4	48 × 52	2.70–11.0	<−20.0	<−0.03	>9.998	<0.30	–	–	FR4
[23] 2021	2 × 2	22 × 22	3.30–3.71	<−12.0	<−0.06	–	<0.30	<−10	–	FR4
[26] 2019	4 × 4	80 × 80	3.18–11.50	<−20.0	<−0.01	>9.98	<0.50	–	–	FR4
P[a]	4 × 4	60 × 60	3.26–5.18	<−15.0	<−0.005	~10.0	<0.05	<−3.0	<−10	FR4

[a]P (proposed antenna).

total reflected power to the total incident power and overall apparent loss". The TARC between any two ports is calculated by

$$TARC_{m\times n} = \sqrt{\frac{(S_{mm} + S_{mn})^2 + (S_{nm} + S_{nn})^2}{2}}, \qquad (19)$$

$$TARC_{14} = \sqrt{\frac{(S_{11} + S_{14})^2 + (S_{41} + S_{44})^2}{2}}. \qquad (20)$$

Figure 8(e) shows the simulated and measured TARC values which are below −10 dB in all the three bands of 5G and the expected values are <0 dB indicating more power is incident rather than reflected and this is due to the highly achieved matched impedance in the proposed design.

Discussion of results and comparison with other state-of-the-art designs

This section discusses the far-field result characterization of the proposed antenna. Figure 9(a) shows the radiation efficiency and measured peak gain (dB) of the proposed antenna. The MIMO antenna offers a radiation efficiency of 0.9 on the normalized scale which is more than 90% in the operating 5G bands. Also, the variation of the peak gain is between 2.50 and 4.50 dBi. Figures 9(b)–9(g) show the 3D radiation pattern which is simulated for 3.50, 4.00, 4.50, 4.80, 3.30, and 5.00 GHz. The 3D radiation pattern shows the capability of the MIMO antenna to maintain desired donut pattern in E- and omni-directional pattern in the H-plane. Figures 9(h)–9(k) show the 2D radiation pattern of the proposed antenna at 3.50, 4.00, 4.50, and 5.00 GHz which shows that all the three 5G bands (n77, n78, and n79) antenna offers dipole-type pattern and omni-directional pattern in both principal planes.

This section also discusses the comparison of the proposed antenna with the present state-of-the-art design which is compared with previously published work and is tabulated in Table 3. It can be observed that the proposed MIMO antenna configuration designed for n77, n78, and n79 5G bands occupies a substantial area of 3364 mm^2 and also utilizes FR4 substrate which makes it a more prominent candidate to be integrated with microwave integrated circuits (MICs) circuits. The comparison table also suggests that the proposed antenna offers very good diversity performance. This novel design of the MIMO antenna makes it more suitable for different handheld devices intended for 5G applications.

Conclusions

In this research article, a 4 × 4 MIMO antenna is proposed where a rectangular stub is used in the ground to achieve isolation and this technique does not only affect the working bandwidth. The Calendula radiating patch which forms the asymmetric fed MIMO antenna configuration offers good diversity performance with ECC < 0.005, DG ~ 10 dB, CCL < 0.05 b/s/Hz, MEG ≈ −3.0 dB, and TARC < −10 dB. The proposed antenna maintains a radiation efficiency of more than 90% and gain between 2.50 and 4.50 dBi. The MIMO antenna is compared with simulated and measured 2D radiation patterns offering excellent dipole-like and omni-directional patterns and desired radiation planes. All the above excellent characteristics offered by the proposed MIMO

antenna make it a suitable candidate for the integration with applications including n77, n78, and n79 bands.

Conflict of interest. None.

References

1. **Hadda L, Sharma M, Gupta N, Kumar S and Singh AK** (2021) On-demand reconfigurable WiMAX/WLAN UWB-X band high isolation 2×2 MIMO antenna for imaging applications. *IETE Journal of Research*, 1–13.
2. **Chandel R and Gautam AK** (2016) Compact MIMO/diversity slot antenna for UWB applications with band-notched characteristic. *Electronics Letters* **52**, 336–338.
3. **Chandel R, Gautam AK and Rambabu K** (2018) Design and packaging of an eye-shaped multiple-input–multiple-output antenna with high isolation for wireless UWB applications. *IEEE Transactions on Components, Packaging and Manufacturing Technology* **8**, 635–642.
4. **Chandel R, Gautam AK and Rambabu K** (2018) Tapered fed compact UWB MIMO-diversity antenna with dual band-notched characteristics. *IEEE Transactions on Antennas and Propagation* **66**, 1677–1684.
5. **Gautam AK, Yadav S and Rambabu K** (2018) Design of ultra-compact UWB antenna with band-notched characteristics for MIMO applications. *IET Microwaves, Antennas & Propagation* **12**, 1895–1900.
6. **Liu L, Cheung SW and Yuk TI** (2013) Compact MIMO antenna for portable devices in UWB applications. *IEEE Transactions on Antennas and Propagation* **61**, 4257–4264.
7. **Liu L, Cheung SW and Yuk TI** (2014) Compact multiple-input–multiple-output antenna using quasi-self-complementary antenna structures for ultrawideband applications. *IET Microwaves, Antennas & Propagation* **8**, 1021–1029.
8. **Liu L, Cheung SW and Yuk TI** (2015) Compact MIMO antenna for portable UWB applications with band-notched characteristic. *IEEE Transactions on Antennas and Propagation* **63**, 1917–1924.
9. **Kaur M and Singh HS** (2021) Design and analysis of high isolated super compact 2 × 2 MIMO antenna for WLAN application. *International Journal of RF and Microwave Computer-Aided Engineering* **31**, 1–14.
10. **Dkiouak A, Zakriti A, El Ouahabi M and McHbal A** (2020) Design of two element Wi-MAX/WLAN MIMO antenna with improved isolation using a short stub-loaded resonator (SSLR). *Journal of Electromagnetic Waves and Applications* **34**, 1268–1282.
11. **Khan MI and Khattak MI** (2020) Designing and analyzing a modern MIMO-UWB antenna with a novel stub for stop band characteristics and reduced mutual coupling. *Microwave and Optical Technology Letters* **62**, 3209–3214.
12. **Pannu P and Sharma DK** (2020) Miniaturize four-port UWB-MIMO antenna with tri-notched band characteristics. *Microwave and Optical Technology Letters* **63**, 1489–1498.
13. **Bhattacharjee A, Karmakar A, Saha A and Bhattacharya D** (2021) Design of a compact UWB MIMO-diversity antenna incorporating fractal inspired isolation structure with band notch characteristics. *Microwave and Optical Technology Letters* **63**, 2597–2605.
14. **Biswas AK, Swarnakar PS, Pattanayak SS and Chakraborty U** (2020) Compact MIMO antenna with high port isolation for triple-band applications designed on a biomass material manufactured with coconut husk. *Microwave and Optical Technology Letters* **62**, 3975–3984.
15. **Sohi AK and Kaur A** (2020) A complementary Sierpinski gasket fractal antenna array integrated with a complementary Archimedean defected ground structure for portable 4G/5G UWB MIMO communication devices. *Microwave and Optical Technology Letters* **62**, 2595–2605.
16. **Xu Y, Wen S and Dong Y** (2021) Compact planar multiple-input-multiple-output antenna with pattern diversity based on the complementary theory. *Microwave and Optical Technology Letters* **63**, 2662–2669.
17. **Kaur H, Singh HS and Upadhyay R** (2021) Design and experimental verification of compact dual-element quasi-self-complementary ultra-wideband multiple-input multiple-output antenna for wireless applications. *Microwave and Optical Technology Letters* **63**, 1774–1780.
18. **Singhal S** (2020) Feather-shaped super wideband MIMO antenna. *International Journal of Microwave and Wireless Technologies* **13**, 94–102.
19. **Vyas K and Yadav RP** (2020) Planar suspended line technique based UWB-MIMO antenna having dual-band notching characteristics. *International Journal of Microwave and Wireless Technologies* **13**, 614–623.
20. **Addepalli T and Anitha VR** (2021) Design and analysis of a novel compact spanner-shaped ultra-wideband antenna for MIMO systems. *International Journal of Communication Systems* **34**, 1–13.
21. **Ibrahim AA and Ali WAE** (2021) High isolation 4-element ACS-fed MIMO antenna with band notched feature for UWB communications. *International Journal of Microwave and Wireless Technologies* **14**, 1–11.
22. **Saravanan M, Kalidoss R, Partibane B and Vishvaksenan KS** (2021) Design of an interlocked four-port MIMO antenna for UWB automotive communications. *International Journal of Microwave and Wireless Technologies* **14**, 1–8.
23. **Sghaier N and Latrach L** (2021) Design and analysis of wideband MIMO antenna arrays for 5G smartphone application. *International Journal of Microwave and Wireless Technologies* **14**, 1–13.
24. **Deng C** (2020) Compact broadband multi-input multi-output antenna covering 3300 to 6000 MHz band for 5G mobile terminal applications. *Microwave and Optical Technology Letters* **62**, 3310–3316.
25. **McHbal A, Amar Touhami N, Elftouh H and Dkiouak A** (2020) Coupling reduction using a novel circular ripple-shaped decoupling mechanism in a four-element UWB MIMO antenna design. *Journal of Electromagnetic Waves and Applications* **34**, 1647–1666.
26. **Hasan MN, Chu S and Bashir S** (2019) A DGS monopole antenna loaded with U-shape stub for UWB MIMO applications. *Microwave and Optical Technology Letters* **61**, 2141–2149.
27. **Karimian R, Soleimani M and Hashemi SM** (2012) Tri-band four elements MIMO antenna system for WLAN and WiMAX application. *Journal of Electromagnetic Waves and Applications* **26**, 2348–2357.
28. **Sharma M, Vashist PC, Ashtankar PS and Mittal SK** (2020) Compact 2 × 2/4 × 4 tapered microstrip feed MIMO antenna configuration for high-speed wireless applications with band stop filters. *International Journal of RF and Microwave Computer-Aided Engineering* **31**, 1–16.
29. **Sharma M, Dhasarathan V, Patel SK and Nguyen TK** (2020) An ultra-compact four-port 4×4 superwideband MIMO antenna including mitigation of dual notched bands characteristics designed for wireless network applications. *AEU – International Journal of Electronics and Communications* **123**, 1–10.
30. **Dhasarathan V, Nguyen TK, Sharma M, Patel SK, Mittal SK and Pandian MT** (2020) Design, analysis and characterization of four port multiple-input-multiple-output UWB-X band antenna with band rejection ability for wireless network applications. *Wireless Networks* **26**, 4287–4302.
31. **Hassan MM, Rasool M, Asghar MU and Zahid Z** (2019) A novel UWB MIMO antenna array with band notch characteristics using parasitic decoupler. *Journal of Electromagnetic Waves and Applications* **34**, 1225–1238.
32. **Rajkumar S, Amala AA and Selvan KT** (2019) Isolation improvement of UWB MIMO antenna utilising molecule fractal structure. *Electronics Letters* **55**, 576–579.
33. **Khan MS, Iftikhar A, Shubair RM, Capobianco AD, Braaten BD and Anagnostou DE** (2020) A four element, planar, compact UWB MIMO antenna with WLAN band rejection capabilities. *Microwave and Optical Technology Letters* **62**, 3124–3131.
34. **Eslami A, Nourinia J, Ghobadi C and Shokri M** (2021) Four-element MIMO antenna for X-band applications. *International Journal of Microwave and Wireless Technologies* **13**, 859–866.
35. **Malaisamy K, Santhi M and Robinson S** (2020) Design and analysis of 4×4 MIMO antenna with DGS for WLAN applications. *International Journal of Microwave and Wireless Technologies* **13**, 979–985.
36. **Shannon CE** (1949) Communication in the presence of noise. *Proceedings of the institute of Radio Engineers* **37**, 10–21.

Dr. Tathababu Addepalli was born in 1986, AP, India. He received his B.Tech. degree from JNTUH, Hyderabad in 2007, M.Tech. degree from JNTUK, Kakinada in 2010, and Ph.D. degree from JNTUA, Anantapur in 2022. Currently, he is working as Associate Professor in the department of ECE at Aditya Engineering College (A), Surampalem, Kakinada, Andhra Pradesh. He has published 10 SCIE research papers in various reputed international journals like Elsevier (*International Journal of Electronics and Communications* (AEU)), Wiley (*International Journal of Communication Systems* (IJCS)), MDPI (*Electronics*), Springer (*Wireless Personal Communications* (WPC)), Wiley (*Transaction on Emerging Telecommunication Technologies* (ETT)), Elsevier (*Alexandria Engineering Journal* (AEJ)), and Taylor & Francis (*Journal of Electromagnetic Waves and Applications*), presented five conferences (four IEEE, one Springer), published two book chapters on THz antennas and planar antennas. He attended more than 40 workshops in various reputed institutions. His areas of interest are microstrip patch antennas, MIMO antennas, 5G antennas, flexible antennas, characteristic mode analysis (CMA), THz antennas, and metamaterial antennas.

Dr. Thota Vidyavathi received her B.Tech. degree from JNTU Hyderabad in the Department of Electronics and Communication Engineering during the year 2006 and the Master of Technology in Radar and Microwave Engineering from Andhra University College of Engineering (A) in the year 2008. Her Ph.D. degree was awarded in the year 2015 from the Department of ECE, Andhra University. Currently, she is working as an Assistant Professor in the Department of ECE, Gayatri Vidya Parishad College of Engineering (A), Visakhapatnam, Andhra Pradesh, India. Her research interests include array antennas, electromagnetic theory and wave propagation, radar engineering, microwave engineering, EMI/EMC, computational electromagnetics, and soft computing. She has guided more than 20 UG and PG projects. She is a member of IEEE antennas and Propagation Society; she is life member of Society of EMC Engineers, SEMCE (India) also a member of International Association of Engineers (IAENG) and International Association of Academic plus corporate (IAAC). She is a Fellow member of IETE. She is recipient of Young Scientist Award-March 2020 and Young Women Researcher Award-February 2022. Presently she is working in the area of array antennas design by using HFSS software simulation. She has three patents and published in various reputed national and international journals. She is paper reviewer for various Scopus and SCI indexed journals. She has organized and coordinated various international conferences, technical workshops, faculty development programs, and given guest lectures in the department.

Neelima Koppala received her M.Tech. degree in Embedded Systems from JNTUA Anantapur in 2015, and is now currently working as an Assistant Professor in ECE Department, Sree Vidyanikethan Engineering College, Tirupati. She has published more than five peer-reviewed journals and presented conferences in various reputed institutions. Her current research interests include MIMO antennas, reconfigurable antennas, information theory, VLSI, and image processing.

Dr. Manish Sharma received B.E. degree in Electronics and Communication Engineering from Mangalore University, Karnataka, India in 2000 and M.Tech. degree from Visvesvaraya Technological University, Karnataka, India in 2007. He completed his Ph.D. degree from the Department of Electronics Engineering, Banasthali University, Rajasthan, India in 2017. He is currently working as a Professor-Research in Chitkara University Research and Innovation Network (CURIN), Chitkara University, Punjab, India. His research interest includes computational electromagnetics, reconfigurable antennas, novel electromagnetic materials, dielectric resonator antennas, wideband/superwideband antennas, wideband/dual band/triple band microstrip antennas for wireless communication, smart and MIMO antennas systems, radio-frequency identification (RFID) antennas, antennas for healthcare, RF MEMS planar antenna on Si substrate, wireless networks, body area networks, meta surface-based biosensors, designing of microstrip antennas using machine learning and artificial network. He has published more than 100+ research articles in SCI/SCOPUS Indexed journals and also granted three patents. He has guided two Ph.D. students and currently there are eight ongoing Ph.D. scholars.

Dr. Dheeraj Kumar received M.Sc. and Ph.D. degrees in Physics. He is currently an Assistant Professor in the Department of Physics and Electronics, Rajdhani College (University of Delhi), Delhi. He has published several scientific papers in the field of microstrip antenna. His research interests include MIMO, 5G antenna system, and terahertz antenna.